第 36 卷第 2 期 无 机 化 学 学 报 Vol.36 No.2
2020 年 2 月 CHINESE JOURNAL OF INORGANIC CHEMISTRY 377-384

由醚氧桥连四羧酸配体构筑的锰(Ⅱ)和锌(Ⅱ)配位聚合物的合成、晶体结构、荧光及磁性质

黎 彧[1] 赵振宇*[,2] 邹训重[1] 冯安生[1] 顾金忠*[,3]
([1]广东轻工职业技术学院,广东省特种建筑材料及其绿色制备工程技术研究中心/佛山市特种功能性建筑材料及其绿色制备技术工程中心,广州 510300)
([2]深圳信息职业技术学院智能制造与装备学院,深圳 518172)
([3]兰州大学化学化工学院,兰州 730000)

摘要:采用水热方法,用醚氧桥连四羧酸配体(H_4L)和菲咯啉(phen)、吡啶(py)分别与 $MnCl_2·4H_2O$ 和 $ZnCl_2$ 反应,合成了 2 个二维配位聚合物$\{[Mn_2(\mu_6\text{-}L)(phen)_2]·5H_2O\}_n$ (**1**)和$\{[Zn_2(\mu_7\text{-}L)(py)]·H_2O\}_n$ (**2**),并对其结构、荧光和磁性质进行了研究。结构分析结果表明 2 个配合物分别属于三斜和单斜晶系,$P\bar{1}$ 和 $I2/a$ 空间群。配合物 **1** 和 **2** 分别具有基于四核锰和双核锌的二维层结构。荧光和磁性研究结果表明,配合物 **2** 在室温下能发出蓝色荧光,聚合物 **1** 中相邻 Mn(Ⅱ)离子间存在反铁磁相互作用。

关键词:配位聚合物;醚氧桥连四羧酸配体;荧光;磁性
中图分类号:O614.71[+]1;O614.24[+]1 **文献标识码**:A **文章编号**:1001-4861(2020)02-0377-08
DOI:10.11862/CJIC.2020.042

Syntheses, Crystal Structures, Luminescent and Magnetic Properties of 2D Manganese(Ⅱ) and Zinc(Ⅱ) Coordination Polymers Based on an Ether-Bridged Tetracarboxylic Acid

LI Yu[1] ZHAO Zhen-Yu*[,2] ZOU Xun-Zhong[1] FENG An-Sheng[1] GU Jin-Zhong*[,3]
([1]*Guangdong Research Center for Special Building Materials and Its Green Preparation Technology/Foshan Research Center for Special Functional Building Materials and Its Green Preparation Technology, Guangdong Industry Polytechnic, Guangzhou* 510300, *China*)
([2]*School of Intelligent Manufacturing and Equipment, Shenzhen Institute of Information Technology, Shenzhen, Guangdong* 518172, *China*)
([3]*College of Chemistry and Chemical Engineering, Lanzhou University, Lanzhou* 730000, *China*)

Abstract: Two 2D manganese(Ⅱ) and zinic(Ⅱ) coordination polymers, namely $\{[Mn_2(\mu_6\text{-}L)(phen)_2]·5H_2O\}_n$ (**1**) and $\{[Zn_2(\mu_7\text{-}L)(py)]·H_2O\}_n$ (**2**), have been constructed hydrothermally using H_4L (H_4L=3,3′,4,5′-diphenyl ether tetracarboxylic acid), phen (phen=1,10-phenanthroline), py (py=pyridine), and manganese or zinc chlorides. Single-crystal X-ray diffraction analyses revealed that two complexes crystallize in the triclinic or monoclinic systems, space groups $P\bar{1}$ or $I2/a$. Both complexes feature a 2D sheet structure based on Mn_4 or Zn_2 subunits. The luminescent and magnetic properties for two complexes were also investigated. The results of fluorescence and

收稿日期:2019-07-26。收修改稿日期:2019-11-06。
广东省高等职业院校珠江学者岗位计划资助项目(2015,2018),广东轻院珠江学者人才类项目(No.RC2015-001),生物无机与合成化学教育部重点实验室开放基金(2016),广东省高校创新团队项目(No.2017GKCXTD001),广州市科技计划项目(No.201904010381),深圳市科技计划项目(No.JCYJ20170817112445033,GGFW2017041209483817),广东省大学生科技创新培育专项(No.pdjh2019b0690),广东轻院科技成果培育项目(No.KJPY2018-010)和广东轻院优秀青年基金项目(No.QN2018-007)资助。
*通信联系人。E-mail:gujzh@lzu.edu.cn,yxpzzy01@163.com

magnetic studies show that complex **2** can emit blue fluorescence at room temperature, and antiferromagnetic interactions exist between adjacent Mn(Ⅱ) ions in polymer **1**. CCDC: 1943370, **1**; 1943371, **2**.

Keywords: coordination polymer; ether-bridged tetracarboxylic acid; luminescent properties; magnetic properties

The design and synthesis of coordination polymers have become the subjects of extensive investigation owing to the intriguing structures and functional properties, such as gas separation, catalysis, sensing, luminescence and magnetism[1-8]. The applications of such functional coordination polymers largely depend on the metal ions, organic ligands, solvent systems, temperatures, and pH values[9-14].

In this context, semi-rigid polycarboxylate ligands have been extensively utilized to synthesize various functional coordination polymers owing to their strong coordination ability in diverse modes and the fact that they are able to satisfy the geometric requirement of the metal centers, which leads to higher dimensional frameworks[10,12,15-19].

In this context, we selected 3,3′,4,5′-diphenyl ether tetracarboxylic acid (H_4L) as an organic linker owing to the following features: (1) it can twist and rotate freely to generate different angles between the two phenyl planes via the C-O_{ether}-C bond to furnish a subtle conformational adaptation; (2) it has nine potential coordination sites (eight carboxylate O donors and one O_{ether} donor), which can lead to diverse coordination patterns and high dimensionalities, especially when acting as a multiply bridging block; (3) this acid block remains poorly used for the generation of coordination polymers. Given these features, the main objective of the present study consisted in the exploration of H_4L as a novel ether-bridged tetracarboxylate block for the assembly of diverse coordination polymers.

In this work, we report the syntheses, crystal structures, luminescent and magnetic properties of two Mn(Ⅱ) and Zn(Ⅱ) coordination polymers constructed from the ether-bridged tetracarboxylate ligand.

1 Experimental

1.1 Reagents and physical measurements

All chemicals and solvents were of AR grade and used without further purification. Carbon, hydrogen and nitrogen were determined using an Elementar Vario EL elemental analyzer. IR spectra were recorded using KBr pellets and a Bruker EQUINOX 55 spectrometer. Thermogravimetric analysis (TGA) data were collected on a LINSEIS STA PT1600 thermal analyzer with a heating rate of 10 ℃·min^{-1}. Excitation and emission spectra were recorded on an Edinburgh FLS920 fluorescence spectrometer using the solid samples at room temperature. Magnetic susceptibility data were collected in the 2~300 K temperature range on a Quantum Design SQUID Magnetometer MPMS XL-7 with a field of 0.1 T. A correction was made for the diamagnetic contribution prior to data analysis.

1.2 Synthesis of $\{[Mn_2(\mu_6\text{-}L)(phen)_2]\cdot 5H_2O\}_n$ (1)

A mixture of $MnCl_2\cdot 4H_2O$ (0.040 g, 0.20 mmol), H_4L (0.035 g, 0.10 mmol), phen (0.040 g, 0.20 mmol), NaOH (0.016 g, 0.40 mmol) and H_2O (10 mL) was stirred at room temperature for 15 min, and then sealed in a 25 mL Teflon-lined stainless steel vessel, and heated at 160 ℃ for 3 days, followed by cooling to room temperature at a rate of 10 ℃·h^{-1}. Yellow block-shaped crystals of **1** were isolated manually, and washed with distilled water. Yield: 54% (based on H_4L). Anal. Calcd. for $C_{40}H_{32}Mn_2N_4O_{14}$ (%): C 53.23, H 3.57, N 6.21; Found(%): C 53.36, H 3.58, N 6.17. IR (KBr, cm^{-1}): 3 389w, 3 066w, 1 610m, 1 565s, 1 515m, 1 448w, 1 427m, 1 381s, 1 258w, 1 220w, 1 142w, 1 103 w, 1 063w, 980w, 847m, 778w, 724m, 634w, 545w.

1.3 Synthesis of $\{[Zn_2(\mu_7\text{-}L)(py)]\cdot H_2O\}_n$ (2)

A mixture of $ZnCl_2$ (0.027 g, 0.20 mmol), H_4L (0.035 g, 0.10 mmol), py (0.50 mL, 6.30 mmol), and H_2O (10 mL) was stirred at room temperature for 15 min, and then sealed in a 25 mL Teflon-lined stainless steel vessel, and heated at 160 ℃ for 3 days, followed by cooling to room temperature at a rate of 10 ℃·h^{-1}. Colorless block-shaped crystals of **2** were isolated manually, and washed with distilled water.

Yield: 50% (based on H_4L). Anal. Calcd. for $C_{21}H_{13}Zn_2NO_{10}$(%): C 44.24, H 2.30, N 2.46; Found(%): C 44.03, H 2.29, N 2.47. IR (KBr, cm^{-1}): 3 562w, 3 495w, 3 076w, 1 630s, 1 571s, 1 448m, 1 386s, 1 298w, 1 265m, 1 220 w, 1 147w, 1 103w, 1 069w, 1 047w, 985w, 935w, 901w, 851w, 834w, 795w, 767w, 718w, 662w, 644w, 584w, 534w.

The complexes are insoluble in water and common organic solvents, such as methanol, ethanol, acetone and DMF.

1.4 Structure determinations

Two single crystals with dimensions of 0.25 mm×0.20 mm×0.19 mm (**1**) and 0.26 mm×0.24 mm×0.23 mm (**2**) were collected at 293(2) K on a Bruker SMART APEX Ⅱ CCD diffractometer with Mo $K\alpha$ radiation (λ =0.071 073 nm). The structures were solved by direct methods and refined by full matrix least-square on F^2 using the SHELXTL-2014 program[20]. All non-hydrogen atoms were refined anisotropically. All the hydrogen atoms were positioned geometrically and refined using a riding model. Disordered solvent molecules in **1** were removed using the SQUEEZE routine in PLATON[21]. The number of solvent water molecules was obtained on the basis of elemental and thermogravimetric analyses. A summary of the crystallography data and structure refinements for **1** and **2** is given in Table 1. The selected bond lengths and angles for complexes **1** and **2** are listed in Table 2. Hydrogen bond parameters of complex **2** are given in Table 3.

CCDC: 1943370, **1**; 1943371, **2**.

Table 1　Crystal data for complexes 1 and 2

Complex	1	2
Chemical formula	$C_{40}H_{32}Mn_2N_4O_{14}$	$C_{21}H_{13}Zn_2NO_{10}$
Molecular weight	902.49	570.06
Crystal system	Triclinic	Monoclinic
Space group	$P\bar{1}$	$I2/a$
a / nm	1.087 55(9)	1.785 54(8)
b / nm	1.182 56(11)	1.319 04(4)
c / nm	1.420 46(11)	1.801 75(6)
α / (°)	75.404(7)	
β / (°)	88.089(7)	92.856(3)
γ / (°)	75.299(8)	
V / nm^3	1.709 1(3)	4.238 2(3)
Z	2	8
F(000)	824	2 288
θ range for data collection	3.428~25.048	3.464~25.048
Limiting indices	$-12 \leqslant h \leqslant 9$, $-14 \leqslant k \leqslant 13$, $-15 \leqslant l \leqslant 16$	$-20 \leqslant h \leqslant 21$, $-15 \leqslant k \leqslant 11$, $-21 \leqslant l \leqslant 20$
Reflection collected, unique (R_{int})	10 937, 6 032 (0.061 7)	13 704, 3 752 (0.040 9)
D_c / ($g\cdot cm^{-3}$)	1.579	1.787
μ / mm^{-1}	0.806	2.324
Data, restraint, parameter	6 032, 0, 496	3 752, 0, 307
Goodness-of-fit on F^2	0.961	1.048
Final R indices [$I \geqslant 2\sigma(I)$] R_1, wR_2	0.072 1, 0.157 2	0.042 1, 0.103 7
R indices (all data) R_1, wR_2	0.121 0, 0.183 6	0.056 1, 0.115 7
Largest diff. peak and hole / ($e\cdot nm^{-3}$)	958 and −719	1 260 and −552

Table 2 Selected bond distances (nm) and bond angles (°) for complexes 1 and 2

1					
Mn(1)-O(1)	0.214 7(4)	Mn(1)-O(6)A	0.205 8(4)	Mn(1)-O(8)B	0.203 4(4)
Mn(1)-N(1)	0.222 3(4)	Mn(1)-N(2)	0.228 5(5)	Mn(2)-O(2)	0.216 3(4)
Mn(2)-O(3)	0.217 5(3)	Mn(2)-O(3)C	0.217 7(4)	Mn(2)-O(9)B	0.214 3(4)
Mn(2)-N(3)	0.229 6(4)	Mn(2)-N(4)	0.229 8(4)		
O(8)B-Mn(1)-O(6)A	110.17(16)	O(8)B-Mn(1)-O(1)	97.57(15)	O(6)A-Mn(1)-O(1)	92.25(15)
O(8)B-Mn(1)-N(1)	122.13(17)	O(6)A-Mn(1)-N(1)	125.62(18)	O(1)-Mn(1)-N(1)	94.61(17)
O(8)B-Mn(1)-N(2)	90.32(17)	O(6)A-Mn(1)-N(2)	93.85(19)	O(1)-Mn(1)-N(2)	167.73(17)
N(1)-Mn(1)-N(2)	73.19(19)	O(9)B-Mn(2)-O(2)	97.62(14)	O(9)B-Mn(2)-O(3)	94.98(14)
O(2)-Mn(2)-O(3)	80.29(14)	O(9)B-Mn(2)-O(3)C	102.45(15)	O(2)-Mn(2)-O(3)C	151.09(14)
O(3)-Mn(2)-O(3)C	77.46(14)	O(9)B-Mn(2)-N(3)	166.85(15)	O(2)-Mn(2)-N(3)	80.40(15)
O(3)-Mn(2)-N(3)	97.48(14)	O(3)C-Mn(2)-N(3)	84.43(15)	O(9)B-Mn(2)-N(4)	96.56(15)
O(2)-Mn(2)-N(4)	107.21(15)	O(3)-Mn(2)-N(4)	165.22(15)	O(3)C-Mn(2)-N(4)	91.03(15)
N(3)-Mn(2)-N(4)	71.89(16)				
2					
Zn(1)-O(1)	0.196 3(3)	Zn(1)-O(7)A	0.192 3(3)	Zn(1)-O(8)B	0.192 2(3)
Zn(1)-N(1)	0.199 8(4)	Zn(2)-O(2)	0.195 7(3)	Zn(2)-O(6)A	0.195 0(3)
Zn(2)-O(4)C	0.191 3(4)	Zn(2)-O(9)B	0.196 6(3)		
O(7)A-Zn(1)-O(8)B	127.52(15)	O(1)-Zn(1)-O(7)A	106.51(15)	O(1)-Zn(1)-O(8)B	106.01(15)
N(1)-Zn(1)-O(7)A	105.44(14)	N(1)-Zn(1)-O(8)B	108.10(14)	O(1)-Zn(1)-N(1)	99.97(15)
O(4)C-Zn(2)-O(6)A	95.08(16)	O(4)C-Zn(2)-O(2)	117.39(17)	O(6)A-Zn(2)-O(2)	112.26(15)
O(4)C-Zn(2)-O(9)B	118.17(18)	O(6)A-Zn(2)-O(9)B	111.88(14)	O(9)B-Zn(2)-O(2)	102.42(15)

Symmetry transformations used to generate equivalent atoms: A: $-x$, $-y$, $-z+1$; B: $x+1$, y, z; C: $-x$, $-y+1$, $-z+1$ for **1**; A: $-x+1$, $-y+1$, $-z+1$; B: $-x+1$, $y+1/2$, $-z+3/2$; C: $-x+1$, $-y+2$, $-z+1$ for **2**.

Table 3 Hydrogen bond lengths (nm) and angles (°) of complex 2

D–H···A	*d*(D-H) / nm	*d*(H···A) / nm	*d*(D···A) / nm	∠DHA / (°)
O(10)–H(1W)···O(3)	0.085 0	0.193 7	0.278 7	178.54
O(10)–H(2W)···O(4)A	0.098 3	0.202 9	0.300 1	169.50

Symmetry code: A: $-x+1$, $-y+2$, $-z+1$.

2 Results and discussion

2.1 Description of the structure

2.1.1 Crystal of $\{[Mn_2(\mu_6\text{-}L)(phen)_2]\cdot 5H_2O\}_n$ (**1**)

An asymmetric unit of complex **1** possesses two Mn(Ⅱ) ions (Mn1 and Mn2), one μ_6-L^{4-} block, two phen moieties and five lattice water molecules (Fig.1). Mn1 center is five-coordinated and reveals a trigonal pyramidal $\{MnN_2O_3\}$ environment, which is completed by three carboxylate O atoms from three μ_6-L^{4-} blocks and a pair of N donors from the phen moiety. The six-coordinated Mn2 ion displays a distorted octahedral $\{MnN_2O_4\}$ geometry filled by four carboxylate O atoms from three μ_6-L^{4-} blocks and a pair of N donors from the phen moiety. The lengths of the Mn-O and Mn-N bonds are 0.203 4(4)~0.217 7(4) and 0.222 3(4)~0.229 8(4) nm, respectively, which are within the normal values for related Mn(Ⅱ) derivatives[10,12,16,19]. The L^{4-} ligand behaves as a μ_6-block (mode Ⅰ, Scheme 1), wherein four deprotonated carboxylate groups adopt monodentate or μ-bridging bidentate modes. In the μ_6-L^{4-} block, a dihedral angle (between two benzene rings) and a C-O_{ether}-C angle are 66.27° and 118.88°, respectively. Four carboxylate groups and two carboxylate

O atoms of four different μ_6-L^{4-} blocks interlink four adjacent Mn(Ⅱ) centers to give a tetranuclear Mn_4 unit (Fig.2). These Mn_4 units are multiply held together by the remaining COO^- groups to generate a 2D sheet (Fig.3).

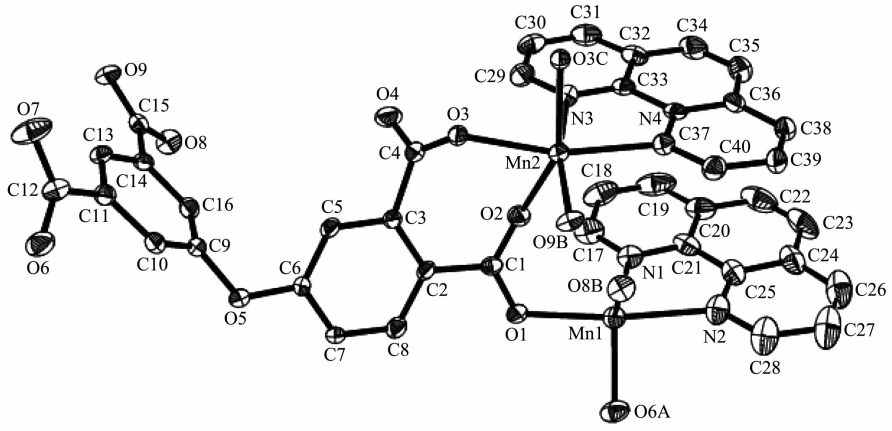

H atoms and lattice water molecules are omitted for clarity; Symmetry codes: A: $-x$, $-y$, $-z+1$; B: $x+1$, y, z; C: $-x$, $-y+1$, $-z+1$

Fig.1　Drawing of asymmetric unit of complex **1** with 30% probability thermal ellipsoids

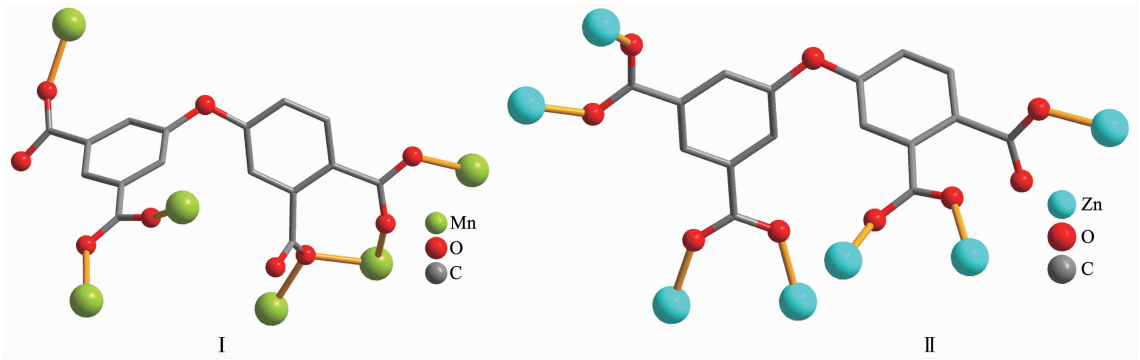

Scheme 1　Coordination modes of L^{4-} ligands in complexes **1** and **2**

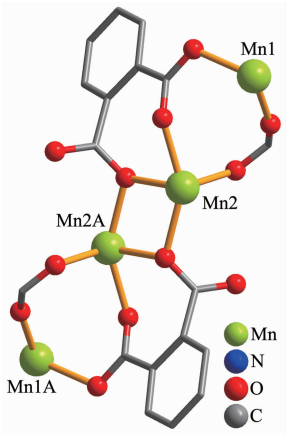

Symmetry code: A: $-x$, $-y+1$, $-z+1$

Fig.2　Tetra-manganese(Ⅱ) subunit in **1**

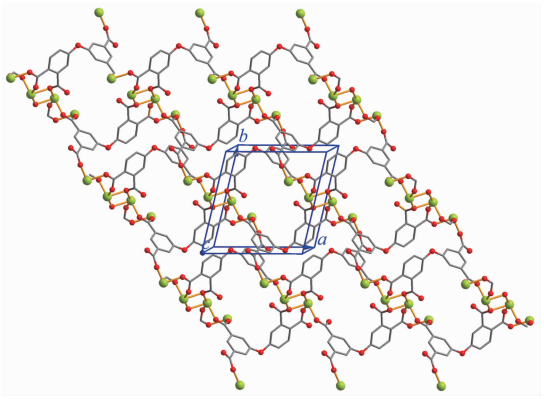

All phen ligands are omitted for clarity

Fig.3　Two dimensional sheet in complex **1** viewed along *c* axis

2.1.2　Crystal of $\{[Zn_2(\mu_7\text{-L})(py)]\cdot H_2O\}_n$ (**2**)

This complex reveals a 2D metal-organic network. An asymmetric unit has two Zn(Ⅱ) ions (Zn1 and Zn2), one μ_7-L^{4-} block, one py ligand and one H_2O molecule of crystallization. The Zn1 center is tetra-coordinated and reveals a distorted tetrahedral $\{ZnNO_3\}$ geometry. It is completed by three carboxylate O donors from three individual μ_7-L^{4-} moieties and one

pyridyl N donor. The Zn2 ion is also tetra-coordinated and has a distorted tetrahedral $\{ZnO_4\}$ environment comprising four carboxylate O atoms of three different μ_7-L^{4-} moieties. The Zn-O (0.191 4(4)~0.196 5(3) nm) and Zn-N (0.199 8(4) nm) bonds are within standard values[12,22-23]. The L^{4-} block acts as a μ_7-linker with its carboxylate groups adopting a monodentate or μ-bridging bidentate mode (mode Ⅱ, Scheme 1). Within the μ_7-L^{4-} block, the dihedral angle between two aromatic rings is 62.07°, whereas the C-O_{ether}-C angle is 118.98°. Two adjacent Zn centers are held together by means of three carboxylate groups coming from three μ_7-L^{4-} spacers (Fig.4). As a result, the dizinc(Ⅱ) subunits with a Zn…Zn separation of 0.332 6(3) nm are formed and further interlinked by μ_7-L^{4-} blocks to produce a 2D network (Fig.6).

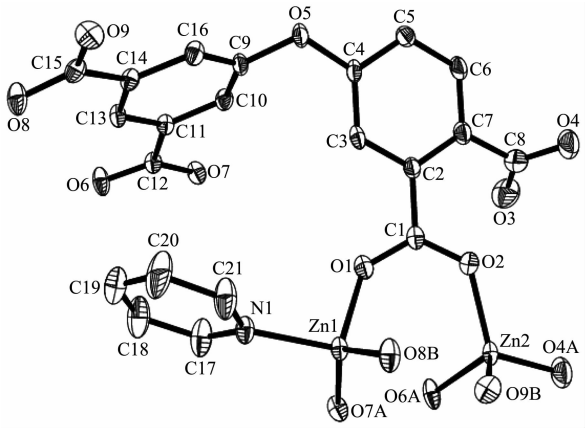

H atoms were omitted for clarity; Symmetry codes: A: $-x+1, -y+1, -z+1$; B: $-x+1, y+1/2, -z+3/2$; C: $-x+1, -y+2, -z+1$

Fig.4 Drawing of asymmetric unit of complex **2** with 30% probability thermal ellipsoids

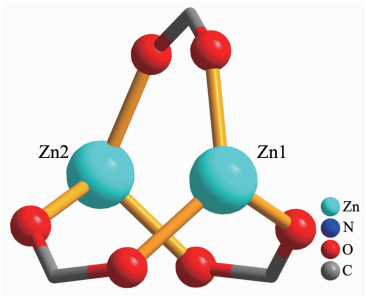

Fig.5 Di-zinc(Ⅱ) subunit in **2**

2.2 TGA analysis

To determine the thermal stability of complexes **1** and **2**, their thermal behaviors were investigated under nitrogen atmosphere by thermogravimetric analysis

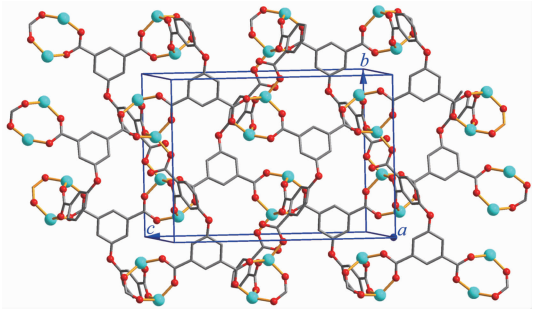

All py ligands and lattice water molecules are omitted for clarity

Fig.6 Two dimensional sheet of **2** viewed along *a* axis

(TGA). As shown in Fig.7, TGA curve of complex **1** shows that there was a loss of five lattice water molecules between 35 and 120 ℃ (Obsd. 9.8%, Calcd. 9.9%); further heating above 220 ℃ leads to a decomposition of the dehydrated sample. Complex **2** lost its one lattice water molecule in a range of 44~142 ℃ (Obsd. 3.1%, Calcd. 3.2%), followed by the decomposition at 392 ℃.

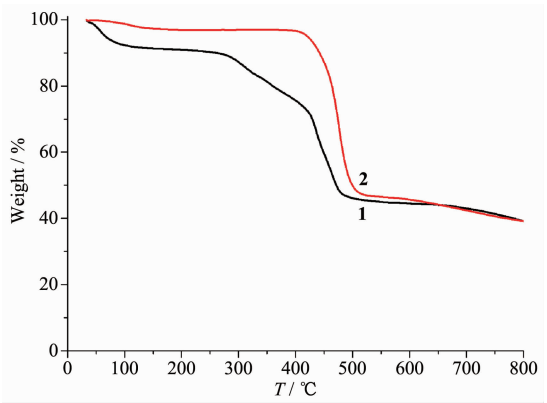

Fig.7 TGA curves of complexes **1**~**2**

2.3 Luminescent properties

Solid-state emission spectra of H_4L and zinc(Ⅱ) complex **2** were measured at room temperature (Fig.8). The spectrum of H_4L revealed a weak emission with a maximum at 467 nm (λ_{ex}=300 nm). In comparison with H_4L, complex **2** exhibited more extensive emission with a maximum at 446 nm (λ_{ex}=300 nm). These emissions correspond to intraligand π-π^* or n-π^* transition of H_4L[10,12,18]. Enhancement of the luminescence in **2** vs H_4L can be explained by the coordination of ligands to Zn(Ⅱ), because the coordination can augment a rigidity of ligands and reduce an energy loss due to radiationless decay[12,18,22].

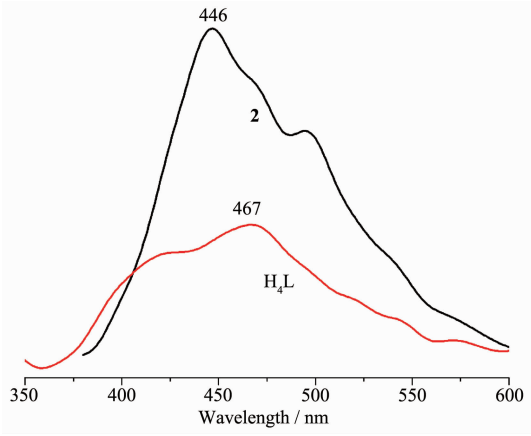

Fig.8　Solid-state emission spectra of H_4L and complex **2** at room temperature

2.4　Magnetic properties

Variable-temperature magnetic susceptibility measurements were performed on powder samples of **1** in the 2~300 K temperature range (Fig.9). For the 2D Mn(Ⅱ) polymer **1** at room temperature, the value of $\chi_M T$, 8.80 $cm^3 \cdot mol^{-1} \cdot K$, was close to the value (8.76 $cm^3 \cdot mol^{-1} \cdot K$) expected for two magnetically isolated high-spin Mn(Ⅱ) ion (S=5/2, g=2.0). If temperature was lowered, the $\chi_M T$ value decreased continuously to a minimum of 1.51 $cm^3 \cdot mol^{-1} \cdot K$ at 2.0 K. Between 10 and 300 K, the magnetic susceptibility can be fitted to the Curie-Weiss law with C=9.50 $cm^3 \cdot mol^{-1} \cdot K$ and θ=−23.22 K. Because of the long separation between the neighboring Mn_4 units, only the coupling interactions within the tetra-manganese(Ⅱ) blocks were considered. A decrease in $\chi_M T$ and a negative θ are due to an overall antiferromagnetic coupling between the manganese centers in the Mn_4 subunits. According to the structure of complex **1** (Fig.2), three are two sets of magnetic exchange pathway within the Mn_4 subunit via two carboxylate O atoms and four carboxylate groups bridges, which could be responsible for the observed antiferromagnetic exchange.

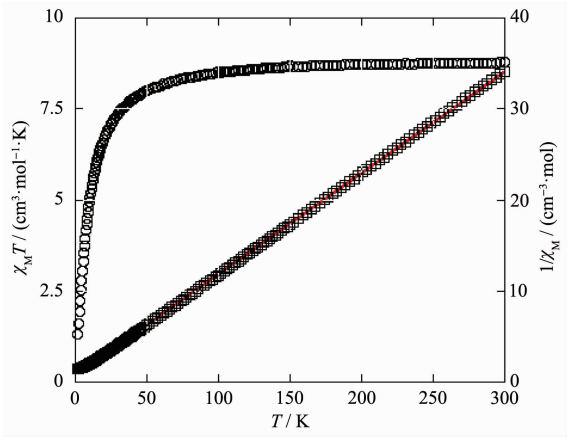

Red line shows the Curie-Weiss fitting

Fig.9　Temperature dependence of $\chi_M T$ (○) and $1/\chi_M$(□) for complex **1**

3　Conclusions

In summary, we have successfully synthesized and characterized two new manganese and zinc coordination polymers by using one unexplored ether-bridged tetracarboxylic acid as ligand under hydrothermal condition. Both complexes feature a 2D sheet structure based on Mn_4 or Zn_2 subunits. Besides, the luminescent (for **2**) and magnetic (for **1**) properties were also investigated and discussed. The results show that such ether-bridged tetracarboxylic acid can be used as a versatile multifunctional building block toward the generation of new coordination polymers.

References:

[1] Zhu J, Usov P M, Xu W Q, et al. *J. Am. Chem. Soc.*, **2018**, **140**:993-1003

[2] Fu H R, Zhao Y, Zou Z, et al. *Dalton Trans.*, **2018**,**47**:3725-3732

[3] Zou L F, Yuan J Q, Yuan Y, et al. *CrystEngComm*, **2019**,**21**:3289-3294

[4] Gu J Z, Wen M, Cai Y, et al. *Inorg. Chem.*, **2019**,**58**:2403-2412

[5] Gu J Z, Wen M, Cai Y, et al. *Inorg. Chem.*, **2019**,**58**:5875-5885

[6] Minguez E G, Coronado E. *Chem. Soc. Rev.*, **2018**,**47**:533-557

[7] Cui Y J, Yue Y F, Qian G D, et al. *Chem. Rev.*, **2012**,**112**:1126-1162

[8] Gao L L, Zhang J, Zhai L J, et al. *J. Solid State Chem.*, **2019**,**271**:346-353

[9] Morrison C N, Powell A K, Kostakis G E, et al. *Cryst. Growth Des.*, **2011**,**11**:3653-3662

[10]Gu J Z, Gao Z Q, Tang Y. *Cryst. Growth Des.*, **2012**,**12**:3312-3323

[11]ZOU Xun-Zhong(邹训重), WU Jiang(吴疆), GU Jin-Zhong(顾金忠), et al. *Chinese J. Inorg. Chem.*(无机化学学报),

2019,**35**(9):1705-1711

[12]Gu J Z, Cui Y H, Liang X X, et al. *Cryst. Growth Des.*, **2016**,**16**:4658-4670

[13]Sánchez-Férez F, Bayés L, Font-Bardia M, et al. *Inorg. Chim. Acta*, **2019**,**494**:112-122

[14]Zhai Z W, Yang S H, Luo P, et al. *Eur. J. Inorg. Chem.*, **2019**:2725-2734

[15]GU Wen-Jun(顾文君), GU Jin-Zhong(顾金忠). *Chinese J. Inorg. Chem.*(无机化学学报), **2017**,**33**(2):227-236

[16]ZHAO Su-Qin(赵素琴), GU Jin-Zhong(顾金忠). *Chinese J. Inorg. Chem.*(无机化学学报), **2016**,**32**(9):1611-1618

[17]Gu J Z, Wen M, Liang X X. *Crystals*, **2018**,**8**:83

[18]Gu J Z, Cai Y, Wen M, et al. *Dalton Trans.*, **2018**,**47**:14327-14339

[19]Yue Q, Liu X, Guo W X, et al. *CrystEngComm*, **2018**,**20**:4258-4267

[20]Spek A L. *Acta Crystallogr. Sect. C*: *Cryst. Struct. Commun.*, **2015**,**C71**:9-18

[21]Van de Sluis P, Spek A L. *Acta Crystallogr. Sect. A*: *Found. Crystallogr.*, **1990**,**A46**:194-201

[22]Gu J Z, Liang X X, Cai Y, et al. *Dalton Trans.*, **2017**,**46**:10908-10925

[23]Chen S S, Sheng L Q, Zhao Y, et al. *Cryst. Growth Des.*, **2016**,**16**:229-241